PHYSICAL REVIEW B VOLUME 24, NUMBER 10 15 NOVEMBER 1981

Electron-spectroscopic studies of $LiNbO_3$ and $LiTaO_3$ surfaces

Victor H. Ritz and Victor M. Bermudez
Optical Sciences Division, Naval Research Laboratory, Washington, D.C. 20375
(Received 11 May 1981)

An analysis is presented of the Auger, uv photoemission, and electron-energy-loss spectra of $LiNbO_3$ and $LiTaO_3$ single-crystal surfaces. Results are reported for the clean surface before and after Ar^+-ion bombardment and for bombarded surfaces after exposure to O_2. Both Ar^+-ion and electron bombardment are found to remove surface oxygen, leading to characteristic changes in the low-kinetic-energy ($\sim 100-250$ eV) Auger spectra. Both materials readily form surface carbides when carbon contamination is present. In uv photoemission, formation of oxygen-ion vacancies by ion bombardment produces a peak above the valence-band edge in both $LiNbO_3$ and $LiTaO_3$. Subsequent exposure to O_2 strongly attenuates the bombardment-induced photoemission. The ultraviolet photoemission spectroscopy (UPS) data are interpreted in terms of M^{4+}—(oxygen vacancy) complexes (M = Nb or Ta). Electron-energy-loss spectroscopy (ELS) data in the 2—90 eV range of loss energies show transitions from the valence band and upper core levels to states in the conduction band. The effects of variation of the primary-beam energy and of O_2 on the intrinsic ELS are examined. Ar^+-ion bombardment results in a low-energy extrinsic ELS peak at $\sim 2.5-3.0$ eV in $LiNbO_3$ and $\sim 3.1-3.5$ eV in $LiTaO_3$. O_2 adsorption has little effect on the loss intensity in $LiNbO_3$ but causes a noticeable decrease in $LiTaO_3$. Annealing at 650 °C, to diffuse Li_2O out of the bulk, diminishes the defect loss peak in $LiNbO_3$ and almost eliminates it in $LiTaO_3$. Defects removed by annealing but not by O_2 adsorption are believed to involve Li^+-ion vacancies. The same low-energy-defect ELS peaks induced by ion bombardment are also observed, with less intensity, in UHV-fractured samples prior to bombardment, and are indicative of a small deficiency of oxygen and lithium. In $LiTaO_3$, a transition at ~ 22 eV, thought to be from the O 2*s* level to the bottom of the conduction band, is observed and found to be dependent on surface oxidation and reduction.

I. INTRODUCTION

The ferroelectric materials $LiNbO_3$ and $LiTaO_3$ are currently being exploited in a wide range of integrated-optic[1] and surface acoustic wave (SAW) devices,[2] and as holographic recording media.[3] Although performance of these devices depends primarily upon the response of the bulk material, some aspects of their operation may be fruitfully studied with the surface and interface-sensitive electron spectroscopies, i.e., Auger (AES), electron-energy-loss (ELS) and ultraviolet photoemission (UPS) spectroscopy. For example, thermally-stimulated desorption ("out-diffusion") of Li_2O from initially stoichiometric $LiNbO_3$ can be used to synthesize guided-wave structures[4] but can present a problem in the high-temperature processing of metal in-diffused devices. Optical damage, a common effect in these materials,[3] is both useful—in that it makes holographic recording possible—and an engineering problem—in that it causes eventual degradation of guided-wave devices at higher power levels. It should be noted that "optical damage" occurs at much lower power levels than "laser damage" in which macroscopic damage results from extremely high power exposures.[5] "Optical damage" results from photoionization of shallow donor levels (e.g., Fe^{2+} impurities). Preferential diffusion of the electrons in a direction parallel to the optic axis, followed by trapping at, for example, Fe^{3+} impurities, produces local microscopic electric fields in the material, which change the extraordinary index of refraction via the electro-optic (Pockels) effect. ELS and UPS are particularly useful in characterizing potential donor and acceptor levels in the optical gap. In addition, some understanding of the effects of electron and ion bombardment on the surfaces of these materials is necessary as a preliminary to the application of surface-analysis methods, such as Auger sputter profiling, to the characterization of devices based on $LiNbO_3$ and $LiTaO_3$ substrates. With these ap-

plications in mind, we have undertaken a study of the AES, ELS, and UPS spectra of undamaged $LiNbO_3$ and $LiTaO_3$ and of Ar^+-ion bombarded surfaces both before and after exposure to O_2.

Some surface investigations have already been carried out on $LiNbO_3$, although none have been reported for $LiTaO_3$. X-ray-photoemission-spectroscopy (XPS) measurements by Steiner and Höchst[6] and by Pearsall *et al.*[7] give the Li *K*-, Nb *M*- and *N*-, and O *K*- and *L*-shell binding energies, as well as an estimate of the electron escape depth as a function of kinetic energy.[6] Steiner and Höchst[6] have also examined the XPS satellite structure, which will be discussed below. Courths *et al.*[8] have studied several aspects of the $LiNbO_3$ surface electronic surface and its response to various perturbations. In XPS, Ar^+-ion bombardment or electron-beam irradiation produces a peak at about 2.4 eV above the valence-band edge. From the concurrent changes in the Nb($3d_{5/2}$,$3d_{3/2}$) core-level XPS lines, the band-gap emission is associated with Nb^{4+} defects. In heavily-damaged samples, traces of Nb^{3+} could be detected in the 3*d* XPS. Changes in surface stoichiometry were followed, using XPS, during annealing via electron-beam irradiation. At present, the relative importance of thermal effects (e.g., Li_2O out-diffusion) and electron-stimulated desorption (ESD) of oxygen is not clear. Initially, Li_2O diffuses out of the bulk until a stoichiometry of approximately $LiNb_3O_8$ is reached. Further removal of oxygen leads to the formation of Nb^{4+}. The observed changes in the relative concentrations of Li^+, Nb^{n+} ($3 \leq n \leq 5$), and O^{2-} imply the presence of electrons trapped in the lattice (in a manner as yet unidentified) in order to maintain charge neutrality. In the case of UPS, Ar^+-ion bombardment also generates a defect peak above the valence-band edge, as well as a change in the shape of the valence-band emission resulting from disorder and/or the creation of oxygen vacancies. However, annealing of the bombarded sample eliminates the defect peak, restoring the original valence-band UPS and producing an ordered low-energy-electron-diffraction (LEED) pattern. This suggests that annealing causes reoxidation of the surface by diffusion of oxygen from the bulk, and is consistent with the observation that exposure to O_2 also removes the UPS defect emission. Recently Kasper and Hüfner[9] have reported the ELS of Ar^+-ion bombarded $LiNbO_3$ before and after annealing, which will be discussed below.

In many respects, $LiNbO_3$ behaves similarly to the much more heavily studied materials TiO_2 and $SrTiO_3$ (Refs. 10—13 and works cited). Both materials can be reduced (i.e., made oxygen deficient) by heating in vacuum or in H_2 or by Ar^+-ion bombardment, causing Ti^{3+} lines to appear in the Ti 2*p* XPS. In UPS, Ar^+-ion bombardment results in surface Ti^{3+}—(oxygen vacancy) complexes which produce a peak at about 2.6 eV above the valence-band edge; these surface defects are removed by O_2 exposure. In TiO_2, as in $LiNbO_3$, annealing of the bombarded (001) and (110) surfaces[13] leads to ordering and reoxidation of the surface. For $SrTiO_3$ (100) and (111) surfaces, on the other hand, annealing orders the Ar^+-ion bombarded surface but does not remove the UPS defect peak. All three materials—$LiNbO_3$, $SrTiO_3$, and TiO_2—become *n*-type semiconducting after annealing at several hundred °C in vacuum.

The object of the present work is a general understanding of the AES, ELS, and UPS of undamaged $LiNbO_3$ and $LiTaO_3$ and of changes in the spectra that occur when defects are introduced by Ar^+-ion bombardment and subsequently removed by O_2 adsorption. Future work will deal with the effect of temperature on surface stoichiometry, the influence of defects on surface electronic structure, and the adsorption of simple gases on $LiNbO_3$ and $LiTaO_3$ with and without defects.

II. EXPERIMENTAL DETAILS

Single-domain crystal boules of $LiNbO_3$ (Curie temperature $T_C \approx 1210$ °C)[1] and $LiTaO_3$ ($T_C \approx 665$ °C) where obtained commerically.[14] The *y* axes were labeled by the supplier and the *z* axes were located by observation through crossed polarizers. The signs of the *x*, *y*, and *z* axes were determined via the piezoelectric effect.[15] According to Kaminow *et al.* (Ref. 15), $LiNbO_3$ cleaves along the (01·2) plane (hexagonal axes), which lies normal to the (*yz*) plane of the crystal, making an angle of 32.75° with the $+z$ axis. For an "ideal," perfectly smooth cleavage face, the crystal could be formally described in terms of alternating Li^+-O^{2-} and Nb^{5+}-O^{2-} planes along the [01·2] axis. Samples were oriented and cut on a diamond saw into blocks $4 \times 4 \times 20$ mm^3 and notches where made so as to initiate cleavage along the (01·2) plane in the UHV system. However, it was found that, with one exception, the samples fractured rather than cleaved in approximately the desired (01·2) orientation. The inability to obtain cleavage may be the

result of residual strain or the fact that the samples were $\sim 4 \times 4$ mm^2 in cross section (x and z dimensions), whereas the specimens of Kaminow *et al.*[15] were only $\sim 0.25 \times 4$ mm^2 in cross section. Although nothing is known about the cleavage properties of $LiTaO_3$, it has the same crystal structure as $LiNbO_3$. Hence, for the sake of consistency, $LiTaO_3$ samples were also prepared in the manner described above.

Most samples were prepared by fracture in UHV ($\lesssim 3 \times 10^{-10}$ Torr) and were electrically insulating. Before being mounted, the samples were coated with an evaporated layer of aluminum a few thousand Å thick to enhance electrical contact with the sample holder. In addition, some experiments were performed on polished plates of $LiNbO_3$ and $LiTaO_3$ of the type used in fabricating integrated-optic devices.[14] The $LiNbO_3$ plates were "y cut" (y axis normal to the plane), and the $LiTaO_3$ samples were "x cut." Only minor differences, except where noted, were found between the results of similar experiments on polished-plate and fractured-crystal surfaces. This indicates that the results reported here are, for the most part, independent of the indices of the surface plane.

The electron spectrometer was a Physical Electronics Model 15-255G double-pass cylindrical-mirror analyzer (CMA). AES measurements were performed in the unretarded first-derivative mode $[d(EN(E))/dE]$, ELS in the retarded first-derivative mode $[dN(E)/dE]$, and UPS (and also some ELS) in the retarded pulse-count mode $[N(E)]$. A 1-V modulation was used in all the derivative spectra. For AES, the resolution was $\Delta E/E \sim 0.4\%$. For ELS, a pass energy of 50 eV was typically used, and the half-width of the elastic peak was in the range $0.8 \leq \Delta E \leq 1.2$ eV. For UPS, a pass energy of 25 eV was used, and the overall resolution was estimated to be better than 0.5 eV. The coaxial electron gun of the CMA provided the primary beam for AES and ELS. Typical beam energies and currents were $E_p = 2.5-3.5$ keV, $i_p = 3$ μA for AES, and $250 \leq E_p \leq 1500$ eV, $i_p = 1.8$ μA for ELS. A sputter-ion gun (Physical Electronics Model 04-181) was used to generate 500-eV Ar^+ ions for bombardment of some of the samples. Usually, 1000-sec exposures were used which removed ~ 120 Å of the surface layer. This corresponded to a particle fluence of $\sim 2 \times 10^{16}$ argon ions/cm^2.

For UPS, a dc-excited He resonance source (Physical Electronics Model 06-180) was used with two-stage differential pumping. During operation of the lamp, the helium pressure in the chamber rose to $\sim 1 \times 10^{-8}$ Torr. All UPS data were obtained with He II excitation ($h\nu = 40.8$ eV), which offers distinct advantages over He I ($h\nu = 21.2$ eV) even though the count rate is about an order of magnitude smaller. The higher excitation energy provides better depth resolution, less overlapping of photoemission structure resulting from "ghost" lines in the source output spectrum and, for the materials of interest, freedom from final-state effects (i.e., conduction-band structure). In regard to the third point, we note that Courths *et al.*[8] observed essentially the same valence band $N(E)$ for excitation at $h\nu = 1486.7$ (Al $K\alpha$) and at 40.8 eV, but a much different $N(E)$ for $h\nu = 21.2$ eV. The analyzer work function was determined to be $\phi_A = 4.25$ eV by observing the Fermi edge of clean gold foil.

In UPS, the positive charge on the sample was "neutralized" via a low-energy-electron flood gun (Physical Electronics Model 04-125). For "neutralized" samples, the UPS charging shift was found to be less than ~ 1 eV by comparison with the data of Courths *et al.*[8] for reduced, semiconducting samples. For AES, in which neutralization was not used, peak energies were reproducible to within ± 1 eV, indicating that the sample charging, although of undetermined magnitude, was constant under nominally constant experimental conditions. The UPS binding energies are referenced to the top of the valence band, because of the uncertainty in the exact value of the charging shift. The position of the top of the valence band was estimated by a linear extrapolation of the upper edge to the point of intersection with the baseline.

Signal averaging, via a Nicolet 1072 Instrument Computer, was used in all experiments. Typically 32 (sometimes 64) 1024-channel sweeps were averaged, with the eV per channel always much less than ΔE. The averaged spectra were recorded on paper tape for further off-line computer processing and plotting. Data reduction sometimes included smoothing[16] and, in the case of UPS, removal of weak "ghost" features[12] resulting from a source line at $h\nu = 48.4$ eV with an estimated intensity of about 7% of that of the He II line.

O_2 exposures were carried out by back-filling the chamber, continuously recording the uncorrected ionization gauge output on a stripchart recorder and graphically integrating the trace. The ionization gauge was not in a direct line of sight to the sample. Exposures are expressed in langmuirs, where 1 L $= 10^{-6}$ Torr sec. This corresponds to a

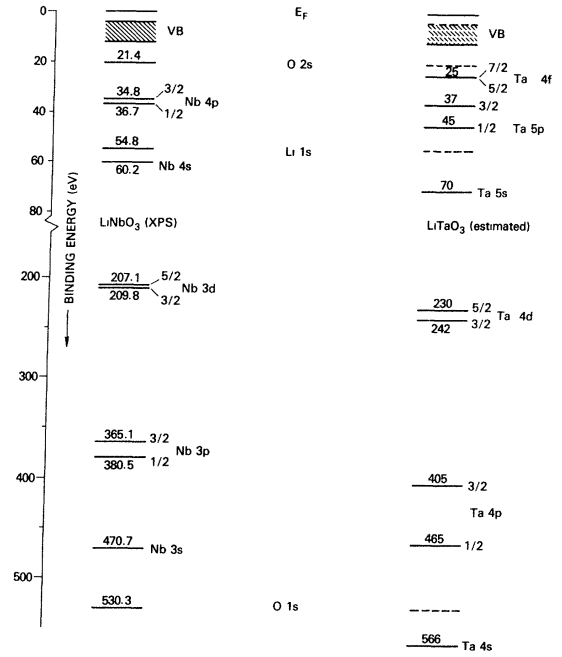

FIG. 1. Energy-level diagrams for $LiNbO_3$ and $LiTaO_3$. The former is derived from XPS data (Refs. 6 and 7) and the latter is estimated as discussed in the text. The placement of E_F near the bottom of the conduction band is appropriate to the n-type semiconducting (i.e., reduced) material.

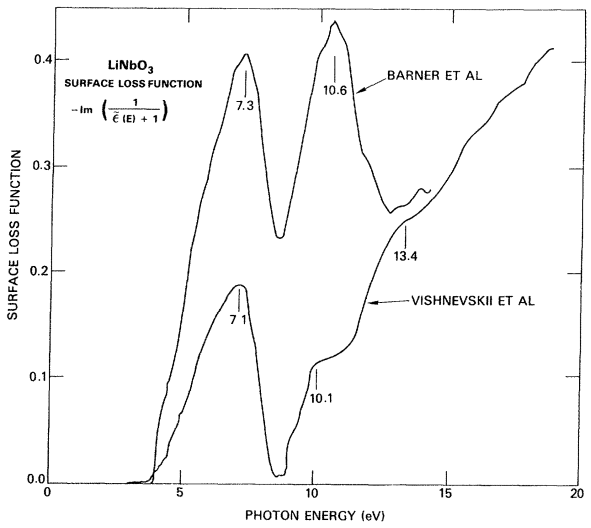

FIG. 2. Surface loss functions computed from the $LiNbO_3$ optical data of Bärner *et al.* (Ref. 19) and of Vishnevskii *et al.* (Ref. 20). The bulk loss function $-\mathrm{Im}[1/\tilde{\epsilon}(E)]$ is also given in Ref. 19.

fluence of $3.59\times10^{14}/\mathrm{cm}^2$ for O_2 at 300 K.[17] A mass-spectroscopic residual-gas analysis of the O_2 indicated only trace amounts of low-molecular-weight impurities. Annealing of the ion-bombarded polished-plate samples was carried out by mounting the specimens on a Ta sheet and using an electron beam heater (Physical Electronics Model 04-121) to irradiate the back of the sheet with $\sim$55 W incident power. The sample itself was not irradiated in this process. The specimen temperature was estimated by means of a Chromel-Alumel thermocouple and an optical pyrometer. The pressure in the chamber rose to $2-5\times10^{-8}$ Torr during annealing.

III. RESULTS AND DISCUSSION

One-electron energy-level diagrams for $LiNbO_3$ and $LiTaO_3$ are shown in Fig. 1; these are useful in analyzing the AES and ELS data. The $LiNbO_3$ diagram is based on the XPS results of Steiner and Höchst,[6] who made efforts to minimize the charging shift. Except for the O 2*s* level, their results agree, within experimental error, with those of Pearsall *et al.*[7] on reduced $LiNbO_3$; however, the latter authors report an O 2*s* binding energy of 17.4 eV. The next level down from O 1*s* is the Nb $2p_{3/2,1/2}$ doublet at about 2371 and 2465 eV, respectively.[18] No comparable XPS data are available for $LiTaO_3$ or for any of the oxides of Ta below the Ta 5*s* level, so the energy-level diagram was approximated by assuming the same Ta core-level energies as in the element[18] and the same Li and O levels as in $LiNbO_3$. Based on a comparison of the Nb core-level energies in the element and in $LiNbO_3$, the Ta binding energies in $LiTaO_3$ are probably underestimated by $\sim$2 eV. The next level down from the Ta 4*s* is the Ta $3d_{5/2,3/2}$ doublet at approximately 1793 and 1735 eV, respectively.

Shown in Fig. 2 is the surface loss function, $-\mathrm{Im}[1/(\tilde{\epsilon}+1)]$, computed from the complex dielectric function, $\tilde{\epsilon}=\epsilon_1+i\epsilon_2$, as measured by Bärner *et al.*[19] and by Vishnevskii *et al.*[20] Both measurements were via normal-incidence reflectance, with the propagation direction normal to the optic axis, the former using nominally unpolarized light and the latter using light polarized normal to the optic axis. The results of Wiesendanger and Güntherodt[21] suggest that the difference between the two loss functions is not the result of crystal anisotropy. Apparently there is considerable, and as yet unexplained, disagreement in the reflectance data above 8 eV.[19–21] This might perhaps result, in part, from variations in sample stoichiometry, since Krol *et al.*[22] find a dependence of the

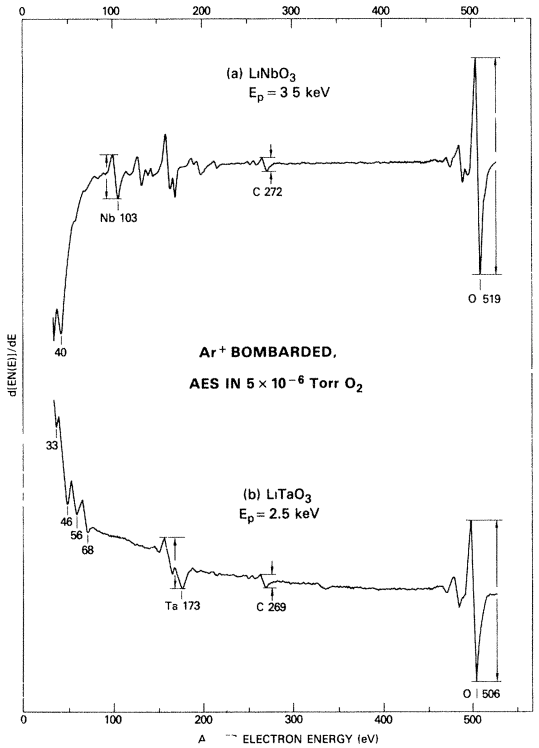

FIG. 3. Auger electron spectra of (a) $LiNbO_3$, $E_p=3.5$ keV, $i_p=3$ μA, (b) $LiTaO_3$, $E_p=2.5$ keV, $i_p=6$ μA. The measurement methods used to obtain the $I_{O(519)}/I_{Nb(103)}$, $I_{O(506)}/I_{Ta(173)}$, $I_{C(272)}/I_{Nb(103)}$, and $I_{C(269)}/I_{Ta(173)}$ peak height ratios are indicated. Both samples were prepared by fracture in UHV, followed by Ar^+-ion bombardment at 500 eV. The spectra were recorded with the samples in an ambient of 5×10^{-6} Torr O_2 (see text).

$LiNbO_3$ optical-absorption edge on composition. The optical gap reported by Bärner *et al.*[19] for $LiNbO_3$ is 3.6 ± 0.1 eV. No optical data in the far-uv are available for $LiTaO_3$, although ϵ_2 vs E has been reported[23] for the cubic perovskite $KTaO_3$ in the 4—14-eV range. The optical gap for $KTaO_3$ (Ref. 23) appears to be ~4 eV.

A. Auger spectra

The AES data for $LiNbO_3$ and $LiTaO_3$ are shown in Fig. 3 and, in more detail, in Figs. 4 and 5. The O*KLL* spectrum in the 480—530-eV range is virtually identical in structure to that in other oxides, reflecting the high degree of localization of the two-hole final state. The remaining AES structure can be analyzed in terms of decay of *M*-shell holes on the niobium ions and *N*-shell holes on the tantalum ions. Inspection of the energy-level diagrams in Fig. 1 shows that Auger decay of holes in the upper core levels (Li *K*, O L_1, etc.) yields transition energies below 50 eV. In keeping with various theoretical estimates[24,25] of relative Auger transition probabilities for intra-atomic and interatomic ("cross-transition") processes, we assume that only holes in the upper core levels of the metal ions will decay by the latter mechanism.

Using the calculated Auger spectra of elemental Nb and Ta, given by Coghlan and Clausing,[18] one can classify various regions of the spectrum as shown for $LiNbO_3$. We are reluctant to identify individual peaks with specific transitions because of uncertainties as to the charging shift, solid-state effects (plasmon and interband loss satellites), and relative intensities which may be distorted in the derivative mode. Nevertheless, certain transitions in $LiNbO_3$ at about 140, 165, and 195 eV fall outside the range of energies for processes involving ejection of only Nb *M*- and *N*-shell electrons. We assign these to transitions involving one or more valence-band (*V*) electrons. The three $LiNbO_3$ AES features are close in energy to the analogous transitions in elemental Nb,[18] defined by substituting "$N_{4,5}$" for "*V*" in Fig. 4(d). For $LiTaO_3$, a qualitative assignment of the AES is more difficult, because of the larger number of possible transitions in a given energy range, and will be discussed below.

AES data for the UHV-fractured $LiNbO_3$ surface, Fig. 4(a), show readily detectable carbon *KLL* transitions in the 240—270-eV range and a strong secondary-electron background which tends to obscure some of the weaker Auger features. Since the level of carbon coverage can be considerably reduced by Ar^+-ion bombardment, the source of the contamination is believed to be decomposition of carbon-containing molecules present in the UHV background, induced by the Auger primary electron beam. Evidently the fresh $LiNbO_3$ surface is very reactive with respect to carbon, since the C*KLL* line shape is that typical of chemically-bound carbon (i.e., a carbide) rather than that of elemental carbon (graphite).[26] Hence, the surface carbon is thought to be present in the form of NbC_x ($x\lesssim1$).

Ar^+-ion bombardment at 500 eV, shown in Fig. 4(b), results in an attenuation of the C*KLL* structure and of the secondary-electron background, a reduction of the surface O-to-Nb ratio and a sharpening of the Auger features. The C*KLL* line shape after ion bombardment is more distinctly "carbidelike" than before, indicating that Ar^+-ion impact may sputter off the elemental ("graphite-

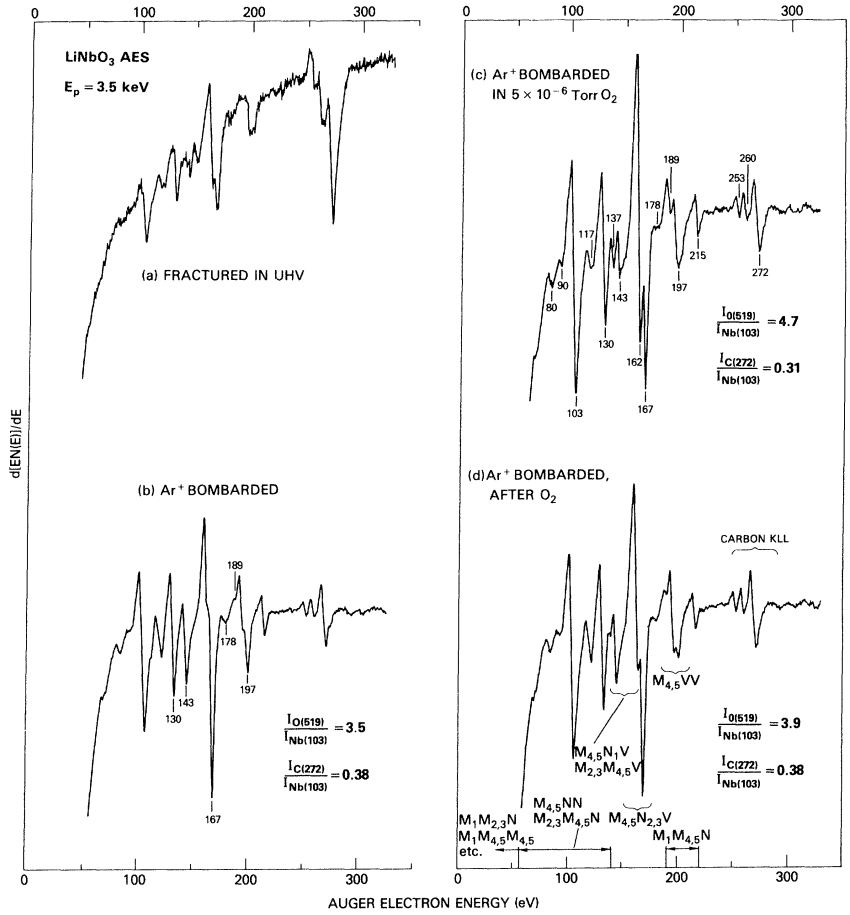

FIG. 4. Detailed Auger electron spectra of $LiNbO_3$, $E_p = 3.5$ keV, $i_p = 3$ μA (a) fractured in UHV, (b) Ar^+-ion bombarded at 500 eV, (c) bombarded sample in 5×10^{-6} Torr O_2, (d) after evacuation of the O_2 background to 5×10^{-9} Torr. The energy ranges in which various types of Auger transitions can occur are indicated. The values of the $I_{O(519)}/I_{Nb(103)}$ and $I_{C(272)}/I_{Nb(103)}$ peak height ratios following the different treatments are given.

like") carbon and/or cause reaction of the oxygen-deficient surface with elemental carbon. Holm and Storp[27] have reported the reaction of carbon with various metal surfaces to form carbides as a result of Ar^+-ion bombardment. AES data for ion-bombarded polished $LiNbO_3$ plates show an even narrower slow secondary peak. Reduction of the sample by ion impact also causes changes in some of the Auger features, which can be seen more clearly by comparing the AES of the bombarded sample before and after O_2 exposure. The peak-to-peak intensity ratio of the O 519-eV and Nb 103-eV lines quantitatively demonstrates the reoxidation of the surface. These particular lines were selected because neither changes shape during the reduction-oxidation cycle. The electron attenuation lengths are estimated[6] to be $\sim$2 Å and $\sim$7 Å at 100 and 500 eV, respectively. Comparison of the spectrum obtained in a background of 5×10^{-6} Torr O_2 with that recorded after evacuation of the O_2 indicates ESD of oxygen by the primary beam. This phenomenon is particularly noticeable in the region of the 162—167-eV doublet. We note that recording the AES in an O_2 background leads to a small reduction in the $I_{C(272)}/I_{Nb(103)}$ peak height ratio, which returns to the initial value after evacuation of the O_2. This probably arises from dissociation of adsorbed O_2 by the electron beam, leading to oxidation of the surface carbide, which is then regenerated during ESD of surface oxygen after evacuation of the O_2. We also note that once the fractured surface has been bombarded to remove the initial carbon contamination, subsequent accumulation of carbon occurs at a much slower rate than for the freshly-fractured surface.

If the AES of the bombarded sample in an O_2

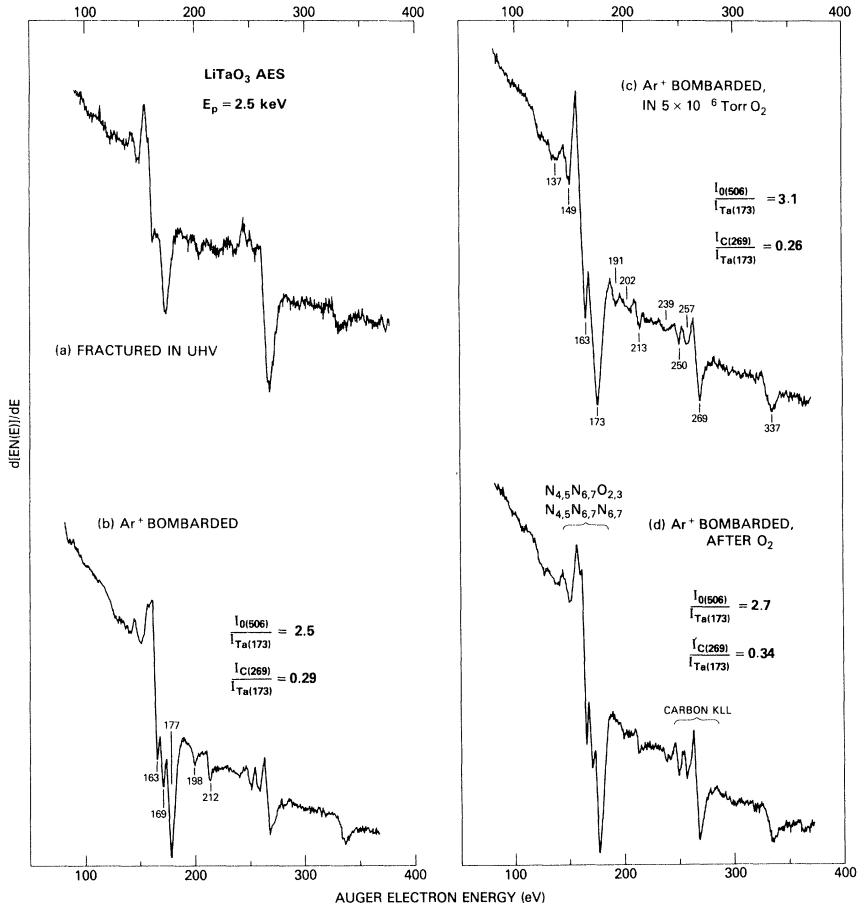

FIG. 5. Detailed Auger electron spectra of $LiTaO_3$, $E_p = 2.5$ keV, $i_p = 6\ \mu A$ (a) fractured in UHV, (b) Ar^+-ion bombarded at 500 eV, (c) bombarded sample in 5×10^{-6} Torr O_2, (d) after evacuation of the O_2 background to 5×10^{-9} Torr. The values of the $I_{O(506)}/I_{Ta(173)}$ and $I_{C(269)}/I_{Ta(173)}$ peak height ratios following the different treatments are given.

ambient Fig. 4(c) is taken to be characteristic of the clean, fully-oxidized surface, the most prominent bombardment-induced changes are in the region of the "valence-band" transitions, $M_{2,3}M_{4,5}V$, etc. Similar effects are seen in the corresponding region of the AES of electron or Ar^+-ion bombarded Nb_2O_5.[28,29] There is an apparent increase in the intensity of the 143-eV peak after bombardment, which may be an artifact of the diminished intensity of the adjacent structures at 137 and 162 eV. It is difficult to distinguish shape changes from intensity changes in the derivative spectra of overlapping transitions. There is also a definite decrease in intensity of the 162-eV line in $M_{4,5}N_{2,3}V$ and of the 189-eV line in $M_{4,5}VV$. The explanation for these effects proposed by Lin and Lichtman,[28] with which we concur, is that they reflect changes in the metal—oxygen chemical bonding near bombardment-induced vacancies. Auger decay of metal-ion core holes is a sensitive probe of local chemical bonding. This is consistent with the fact that Auger transitions involving only core electrons are much less affected by ion impact. The AES of Ar^+-ion bombarded polished plates was closely similar to that shown in Fig. 4(b).

AES data for UHV-fractured $LiTaO_3$ are shown in Fig. 5. The results are qualitatively similar to those for $LiNbO_3$. Before 500-eV Ar^+-ion bombardment, a relatively strong carbidelike $CKLL$ line shape was observed. Bombardment resulted in a decrease in the surface carbon contamination, a more carbidelike $CKLL$ line shape for the remaining carbon and sharper Auger features. Subsequent re-oxidation of the surface showed that ion impact had decreased the surface O-to-Ta ratio. The AES obtained in a background of 4×10^{-6} Torr O_2 after bombardment, is taken to represent that of a clean fully-oxidized surface. As in the case of $LiNbO_3$, the bombarded surface is probably also Li deficient, but Auger decay of Li K-shell holes cannot yield

structure above ~40 eV. After evacuation of the O_2 ambient, the AES showed a partial return to the previous, freshly-bombarded state, indicating ESD of surface oxygen.

Changes in the AES resulting from the oxidation-reduction cycle were observed in the 160–175-eV and 190–215-eV ranges. Reoxidation of the bombarded surface causes an *apparent* decrease in the 169-eV peak. This might actually result from a shape change, since the 176-eV peak is broader and lower in energy (173 eV) after bombardment. After reoxidation, the 198-eV peak in the bombarded specimen is replaced by two weak features at ~191 and 202 eV. Based on the computed[18] values for Ta metal and on the work of Lin and Lichtman[30] on WO_3 and oxidized Ta foil, the 160–175-eV region is attributed to overlapping $N_{4,5}N_{6,7}O_{2,3}$ and $N_{4,5}N_{6,7}N_{6,7}$ transitions. The assignment of the rest of the spectrum is uncertain. The reduction-oxidation induced changes in the 160–175-eV range for $LiTaO_3$ closely resemble those in the corresponding region of WO_3 during ESD of oxygen, but are qualitatively different from those for oxidized Ta foil during ESD. For the W and Ta compounds, the changes in AES have been attributed[30] to core-level binding-energy shifts. Additional low-energy Auger structure was observed at about 33, 46, 56, and 68 eV and found to be essentially independent of the oxidation-reduction cycle. The AES of polished $LiTaO_3$ plates after Ar^+-ion bombardment was similar to that in Fig. 4(b), except that the slow-secondary peak was somewhat narrower.

B. uv photemission spectra

The UPS data for $LiNbO_3$ and $LiTaO_3$ are shown in Figs. 6 and 7. The data in Figs. 6(a) and 7(a) were obtained on freshly-fractured surfaces prior to any electron beam exposure. Before 500-eV Ar^+-ion bombardment, the valence-band energy

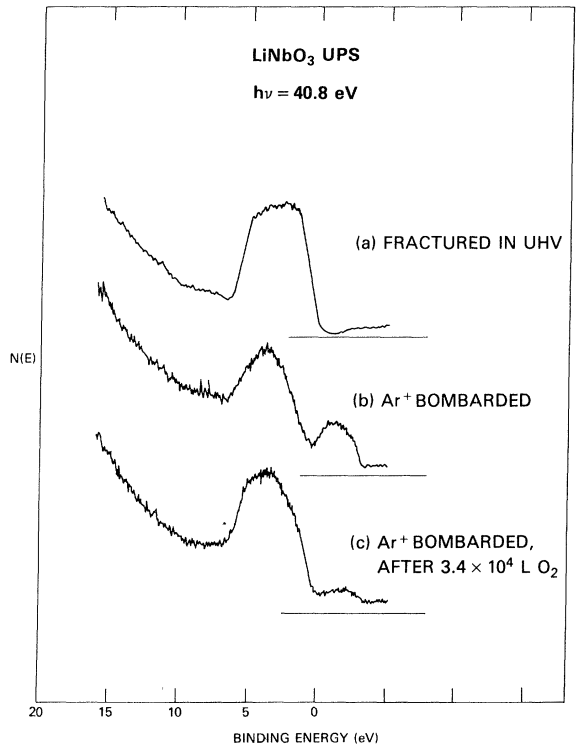

FIG. 6. uv photoemission spectra of $LiNbO_3$, $h\nu$=40.8 eV. Binding energies are referenced to the top of the valence band, with an absolute accuracy of ±0.2 eV. Weak structure occurring above the valence-band edge results from a "ghost" line in the source spectrum at 48.4 eV. The zero count level is indicated by the horizontal lines. (a) Fractured in UHV, (b) Ar^+-ion bombarded at 500 eV, (c) bombarded sample exposed to 3.4×10^4-L O_2.

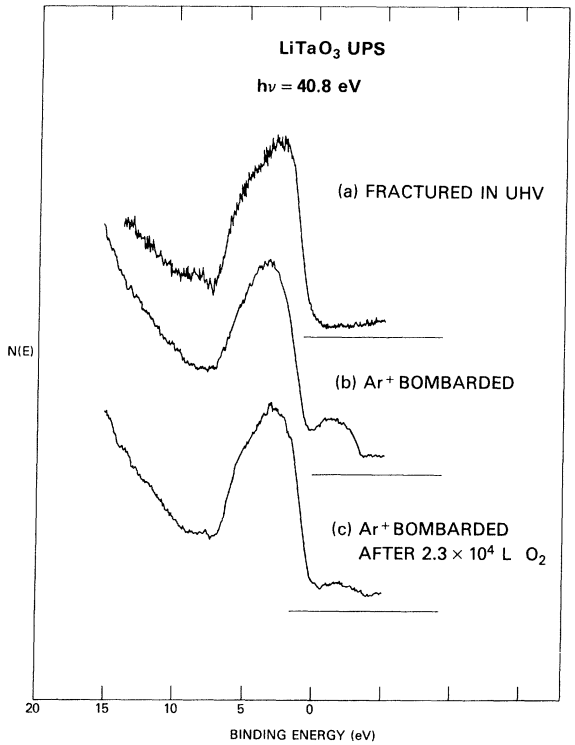

FIG. 7. uv photoemission spectra of $LiTaO_3$, $h\nu$=40.8 eV. (a) Fractured in UHV, (b) Ar^+-ion bombarded at 500 eV, (c) bombarded sample exposed to 2.3×10^4-L O_2.

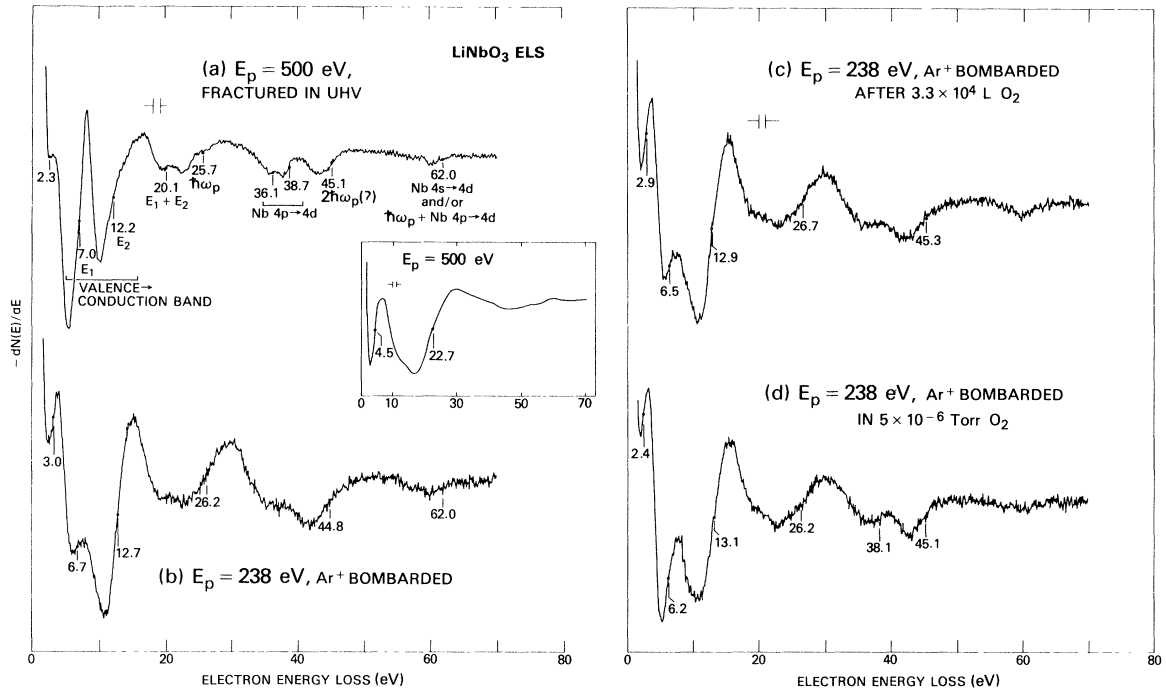

FIG. 8. Electron-energy-loss spectra of $LiNbO_3$ at $E_p = 500$ eV [(a), inset], and at $E_p = 238$ eV (b)–(d). (a) Fractured in UHV, (b) Ar^+-ion bombarded at 500 eV, (c) bombarded sample after an O_2 exposure of about 3×10^4 L, (d) bombarded sample in 5×10^{-6} Torr O_2 background. The peak assignments, which are discussed in the text, are indicated in (a). The inset in Fig. 8 shows a sample fractured in UHV, with possible carbon contamination.

distribution curve (EDC) was similar to that observed by Courths *et al.*[8] in the XPS of undamaged $LiNbO_3$. No previous UPS or XPS data are available for $LiTaO_3$. After bombardment, the valence-band EDC's of both materials appeared more symmetrically peaked, although a detailed study of the shape changes was not performed. A bombardment-induced emission band appeared at about 1.1 eV above the valence-band edge in $LiNbO_3$ and at about 1.4 eV above the edge in $LiTaO_3$. The former result is smaller than that of Courths *et al.*,[8] ~2.3 eV. In accord with the arguments advanced by Courths *et al.*,[8] these features are associated with M^{4+}–(oxygen vacancy) complexes (M = Nb or Ta). In some cases, a very weak peak could be detected in the $LiNbO_3$ UPS at about 6.5 eV below the valence-band edge after ion bombardment.

After an O_2 exposure of about 3×10^4 L, the defect peak was strongly attenuated in both $LiNbO_3$ and $LiTaO_3$, and the valence-band EDC showed a partial return to that of the undamaged sample. The small residual defect peak is believed to result from damage sites lying beyond the depth accessible to the O_2 but within the depth resolution (a few Å) of the UPS experiment.

C. Electron-energy-loss spectra

The $LiNbO_3$ and $LiTaO_3$ ELS results, obtained under a variety of experimental conditions, are shown in Figs. 8–10. For either material, we will discuss the intrinsic losses first (those above ~4 eV), then consider the defect structure. The $LiNbO_3$ ELS, Fig. 8(a), shows two interband transitions, E_1 and E_2, in the 6.5–7.0- and 12.2–12.9-eV ranges and a bulk plasmon loss, $\hbar\omega_p$, in the 25.5–26.7-eV range. The latter result is consistent with the plasmon energy in materials such as $SrTiO_3$ (29.7 eV),[31] $BaTiO_3$ (27.3 eV),[31] and BaO (27.5 eV).[32] A lower limit to the $LiNbO_3$ plasmon energy, $\hbar\omega_p > 18$, is obtained by inspection of the optically-measured loss functions in Fig. 2. A pair of lines occurring at about 36.1 and 38.7 eV is of the correct energy to be assigned to transitions from Nb 4p to Nb 4d (conduction band) states (see Fig. 1). A very weak feature at about 62 eV is likewise assigned to the parity-forbidden Nb 4s $\rightarrow$4d transition. A double-loss transition coupling $\hbar\omega_p$ and Nb 4$p \rightarrow$4d is also possible at this energy. Other loss transitions occur at about 20 and 45 eV. The former is very weak and may be a double-loss involving E_1 and E_2. The latter is somewhat diffi-

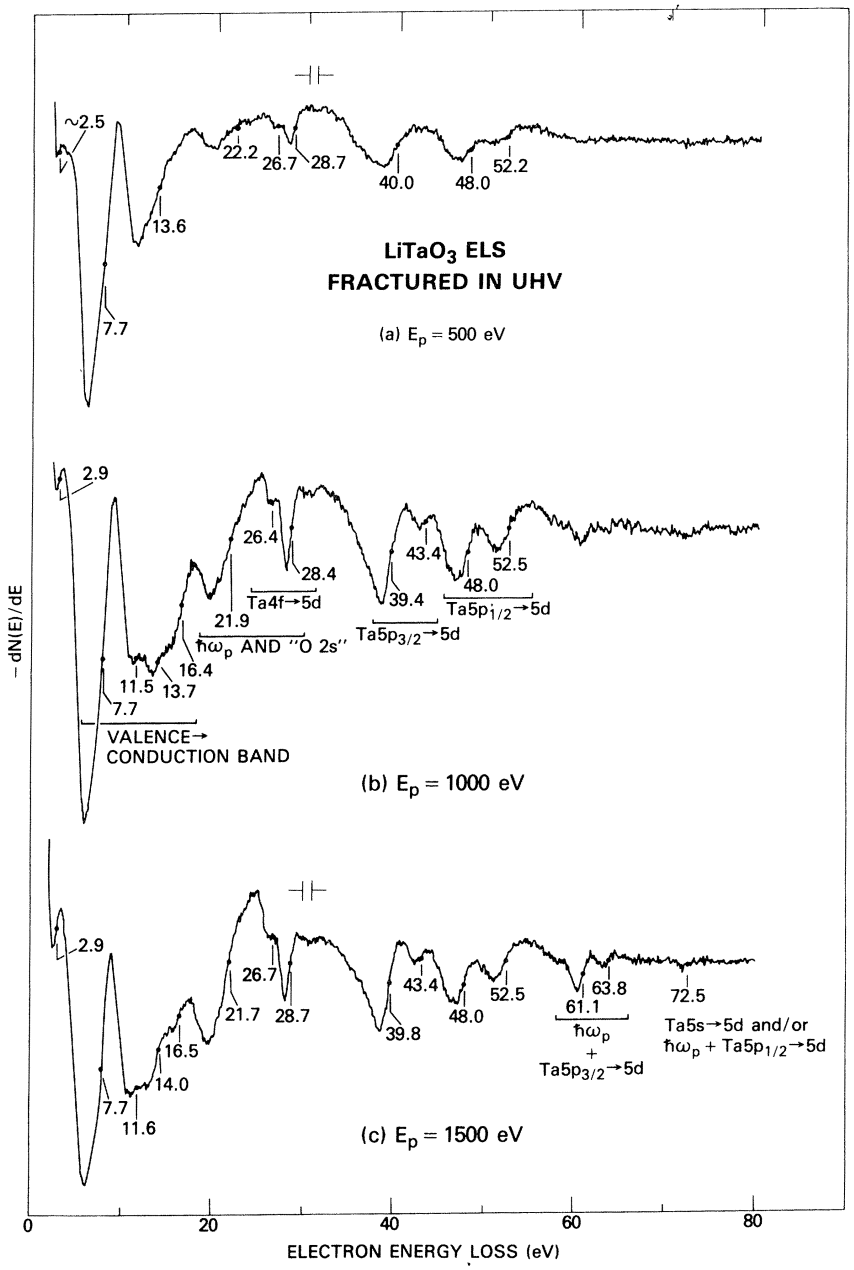

FIG. 9. Electron-energy-loss spectra of $LiTaO_3$ at different values of E_p. The sample was prepared by fracture in UHV. Some of the assignments which are discussed in the text are indicated.

cult to assign. The width and intensity of this feature suggest a double plasmon loss, but it occurs at about 6 eV less than $2\hbar\omega_p$. This 6-eV energy difference may represent the interaction energy of two plasmons in a ferroelectric medium.

Some variation is noted in the interband transition energies from one experiment to the next, as reflected in the ranges of values quoted for E_1 and E_2. These variations are not much larger than the experimental uncertainty; however, the $LiNbO_3$ band-structure calculation of Kam *et al.*[33] shows a high degree of dispersion in the upper part of the valence band and lower part of the conduction band. Some dependence of the interband transition energies on the scattering angle is, therefore, possible if the optical selection rule ("vertical transitions in $\vec{k}$ space") is relaxed somewhat in ELS. Given the irregularity of the fracture surfaces, this might

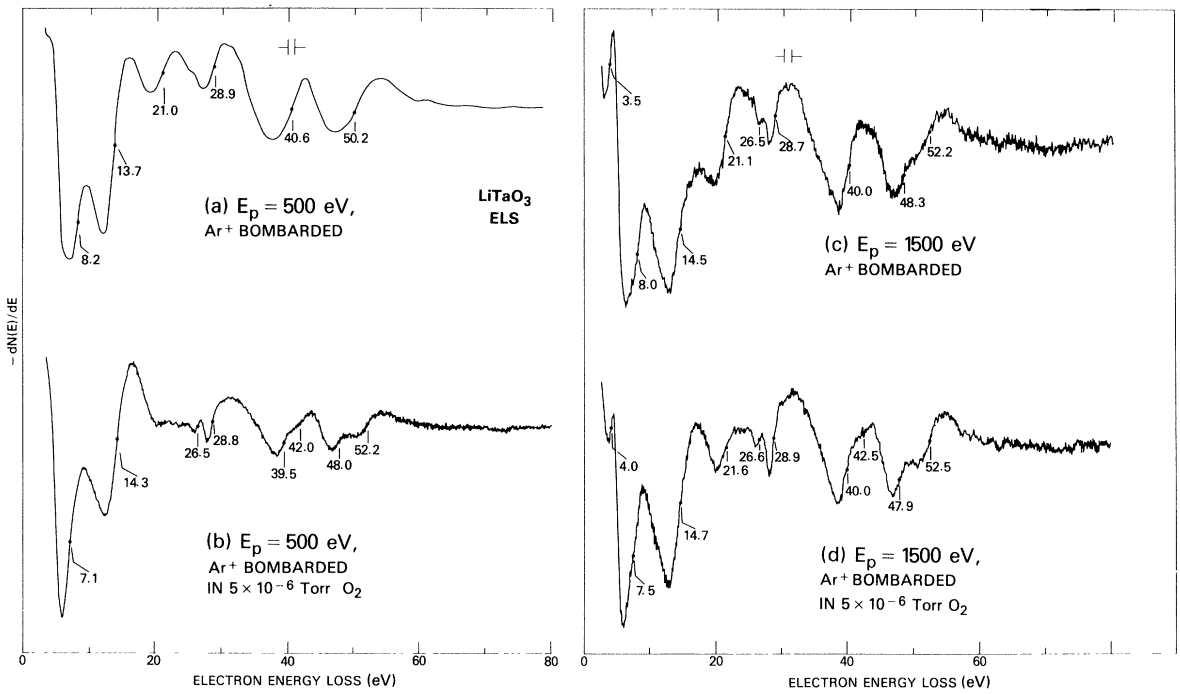

FIG. 10. The effect of O_2 on the $LiTaO_3$ ELS obtained at different values of E_p. The sample was prepared by fracture in UHV followed by Ar^+-ion bombardment at 500 eV. (a) and (b) $E_p = 500$ eV in UHV and in 5×10^{-6} Torr O_2, respectively. (c) and (d) $E_p = 1500$ eV, in UHV and in 5×10^{-6} Torr O_2, respectively.

account for the small variations in E_1 and E_2. Variation of the primary beam energy in the range $240 \lesssim E_p \lesssim 1000$ eV (4 Å $\lesssim$ electron attenuation length $\lesssim 15$ Å)[6] had essentially no effect on the spectra other than a sharpening of some of the lines, particularly E_2 and $\hbar\omega_p$. Hence, any surface-state transitions that might occur are indistinguishable from bulk processes. Uses of E_p outside this range led to serious charging effects.

It is interesting to compare Fig. 8(a) with the optical loss function (Fig. 2), the XPS satellite data of Steiner and Höchst,[6] and the ELS results of Kasper and Hüfner.[9] E_1 is close to the lower optical peak at 7.3 eV, but E_2 does not correlate well with the optical data. The "ELS" of Ref. 6, showing peaks at 7.5, 13.2, and 23.5 eV, was obtained as satellite structure on the high-binding-energy side of the O 1*s* and Nb 3*d* XPS lines. It was assumed that all three peaks were generated by inelastic scattering of the core-level photoelectrons rather than through "shake-up" effects. "Shake-up satellites," which have been studied extensively in TiO_2 and $SrTiO_3$,[34] arise from interband transitions induced by the electronic relaxation of the system in response to the presence of the core hole. The 23.5-eV ELS peak is almost certainly assignable to the bulk plasmon, although it is ~ 2 eV lower than the value of $\hbar\omega_p$ obtained here. At present, it is not clear whether the other peaks are loss features or shake-up satellites. The ELS data of Kasper and Hüfner[9] were obtained with $25 \lesssim E_p \lesssim 130$ eV in the undifferentiated [$N(E)$ vs E] mode using samples that had been Ar^+-ion bombarded and annealed (and, therefore, were semiconducting). A relatively narrow peak was observed at 7.1 eV, and two broad features were found in the 11—13- and 22—24-eV ranges, the former appearing as a poorly-resolved doublet in some spectra. These results are in overall qualitative agreement with those reported here.

We also recorded the undifferentiated ELS at $E_p = 500$ eV in the pulse-count mode, and observed all the structure reported in Fig. 8(a), including the weak loss peaks at 2.3, 20.1, and 62.0 eV. However, the Nb $4p \rightarrow 4d$ transitions appeared as a single unresolved feature in $N(E)$.

Some $LiNbO_3$ ELS data, obtained prior to Ar^+-ion bombardment, appeared as shown in the inset in Fig. 8. There is a single "interband" transition in the anomolously low range of 4.5—6.5 eV (cf. Fig. 2) and a very broad (~ 15 eV half-width) and intense "plasmon" loss at 21.8—23.2 eV. On one sample, both types of spectra [as shown in Fig. 8(a) and in the inset in Fig. 8] were obtained when the

sample was moved so the CMA electron beam struck different points on the surface. Since the data shown in the inset were never obtained after Ar^+-ion bombardment, it is believed that the results are in some way related to the presence of surface carbon, which may be especially concentrated on certain parts of the surface. We do not, at present, understand the exact mechanism whereby the carbon perturbs the ELS. In one series of experiments on a $LiNbO_3$ sample prior to Ar^+-ion bombardment the spectrum in Fig. 8(a) was obtained for $E_p \geq 500$ eV and that in the inset for $E_p \leq 300$ eV. Since the insulating samples often charge at $E_p \leq 250$ eV, this suggests that carbon can affect the ELS through enhancement of the surface charging.

Figs. 8(b)—(d) show the $LiNbO_3$ ELS after Ar^+-ion bombardment at 500 eV and the effects of subsequent O_2 exposure. Bombardment produces a loss peak at about 3.0 eV, while leaving most of the spectrum essentially unchanged. The E_1 interband transition shows an apparent decrease in intensity and a small shift to lower energy. A similar effect is observed in $LiTaO_3$ and will be discussed shortly. We believe that this results from the introduction of disorder and oxygen vacancies and from the overlapping defect peak. The plasmon loss peak is also somewhat sharper after bombardment. In contrast to the results obtained in UPS, Fig. 6, an exposure to O_2 of $\sim 3\times 10^4$ L has no effect on the defect ELS, probably indicating ESD of the adsorbed oxygen by the ELS primary beam, as was observed in the AES data (Fig. 4). Recording the spectrum in a background of 5×10^{-6} Torr O_2 partially restores the E_1 transition. There appears to be no significant decrease in the intensity of the defect loss peak. *The fact that reoxidation of the bombarded sample does not eliminate the* ELS *defect peak means that this center is fundamentally different from that seen in* UPS. A reasonable interpretation is that the defect observed in ELS involves a Li^+-ion vacancy, possibly in association with other types of defects, whereas, the species detected in UPS consist of only Nb^{4+} ions and O^{2-} vacancies. A similar loss peak, in the 2.3—2.5-eV range, is found in the ELS of UHV-fractured samples before Ar^+-ion bombardment, as shown in Fig. 8(a). The intensity of this peak varies somewhat across the sample surface, and recording the spectrum in a background of 5×10^{-6} Torr O_2 has no significant effect on the energy or intensity of this feature. Hence, the bombardment-induced defects observed in ELS are present, to a small extent, on the UHV-fractured surface, which implies that such a surface does not have a fully "ideal" stoichiometry. Since an O_2 background has no significant effect on the ELS (at $E_p = 500$ eV) before ion bombardment, damage by the ELS primary beam through ESD of lattice oxygen can be eliminated as the source of these intrinsic defects.

We have attempted to correlate the ELS data with optical absorptions in $LiNbO_3$ containing various defects.[35—41] In heavily reduced $LiNbO_3$, the Nb^{4+} d-shell transition $[(4d)^1 t_{2g} \rightarrow e_g]$ has been reported by Bollman and Gernand[35] at 2.57 eV by Clark *et al.*[36] at 2.48 eV, somewhat too low in energy to be associated with the 3.0 eV loss peak observed before admission of O_2. In neutron, x-, or gamma-irradiated $LiNbO_3$ (Refs. 37—39 and 41), several optical absorptions are observed in the 2.5—3.5-eV range, but the assignments to specific defects are uncertain. Furthermore, because ion bombardment, unlike low-energy ionizing radiation, is capable of directly displacing lattice ions, the defect observed here might not correspond to any of those formed by x or gamma irradiation. The simplest model for the defect remaining after O_2 adsorption would be a Li^+-ion vacancy adjacent to an O^- ion.

The ELS data for $LiTaO_3$ are shown in Figs. 9 and 10. Figure 9 shows the effects of variation of the primary beam energy and Fig. 10 the results of other treatments. The general features of the spectra can be assigned with the aid of the energy-level diagram in Fig. 1. The complexity of the $LiTaO_3$ spectrum, in comparison with that of $LiNbO_3$, follows from the presence of parity-allowed $p \rightarrow d$ *and* $f \rightarrow d$ transitions and the larger spin-orbit splitting of the Ta $5p$ and $5d$ levels versus the Nb $4p$ and $4d$. Thus the pair of lines at ~ 39.4 and 43.4 eV is of the correct energy for transitions from the Ta $5p_{3/2}$ level to Ta $5d$ levels at the bottom of the conduction band. The pair of lines at ~ 8.5 eV to higher energy is assigned to similar transitions from the Ta $5p_{1/2}$. The pair of lines at ~ 26.4 and 28.4 eV is assigned to transitions from the Ta $4f_{5/2}$, $4f_{7/2}$ doublet (split by about 2 eV)[18] to Ta $5d$ states. At higher E_p there is also a pair of lines at about 61.1 and 63.8 eV. The increase in intensity with E_p suggests the involvement of a bulk plasmon, and these features are assigned to double losses combining $\hbar\omega_p = 21.7$ eV (see below) and Ta $5p_{3/2} \rightarrow 5d$. The extremely weak feature at ~ 73 eV could be the parity-forbidden Ta $5s \rightarrow 5d$ transition or a double-loss combining $\hbar\omega_p$ and

Ta $5p_{1/2} \rightarrow 5d$. We also note in passing the fact that the "sharp" Ta $4f \rightarrow 5d$ transitions are overlapped by the broad plasmon "continuum" centered near $\hbar\omega_p = 21.7$ eV. This raises the interesting possiblity of Fano antiresonance, which is often observed in optical spectra when two excited states involved in overlapping "sharp" and "broad" transitions, respectively, are coupled by some perturbation (see, for example, Refs. 42, 43, and works cited). In this case, the coupling between the $4f \rightarrow 5d$ exciton and the plasmon would originate in the perturbation of the core screening by the $4f$ hole. Further investigation of this point would require careful measurement of the complex dielectric function via optical reflectance. We also note that spectra [$N(E)$ vs E] recorded in the undifferentiated (pulse count) mode showed the same structure as those in Fig. 9 except that the $4f \rightarrow 5d$ and $5p \rightarrow 5d$ doublets all appeared as broad unresolved features.

Within experimental uncertainty, the energies of the $4f \rightarrow 5d$ and $5p \rightarrow 5d$ transitions are independent of E_p and of various surface treatments, although Ar^+-ion bombardment causes broadening of the ELS features and loss of the weaker peaks. However, there is noticeable dependence on E_p in the 13—22-eV part of the spectrum. At low E_p, a broad intense and asymmetric band is seen at ~ 13.6 eV. Increasing E_p makes this feature sharper and slightly higher in energy, revealing very weak structure near ~ 11 and ~ 14 eV. Concurrently, the ~ 22-eV structure becomes sharper and/or more intense with increasing E_p. We assign this latter feature to the bulk plasmon at $\hbar\omega_p = 21.7$ eV, somewhat lower in energy than that for $LiNbO_3$. This value of $\hbar\omega_p$ is consistent with the energies of the double-loss transitions at about 61.1 and 63.8 eV, as noted previously.

We next consider the effects of an O_2 background (4×10^{-6} Torr) on the ELS of an Ar^+-ion bombarded sample, as shown in Fig. 10. Comparison of Figs. 9(a) and 10(a) and of 9(c) and 10(c) shows that bombardment enhances the defect peak at ~ 3.5 eV (to be discussed below), broadens and attenuates the 7.7-eV interband loss peak and broadens the $4f \rightarrow 5d$ and $5p \rightarrow 5d$ peaks. There are also some bombardment-induced shape changes in the 12—25-eV range, but these are difficult to define precisely in derivative spectra. In the surface ELS ($E_p = 500$ eV) after bombardment, O_2 appears to attenuate the ~ 22-eV loss peak. In the bulk ELS ($E_p = 1500$ eV), this peak is also attenuated by an O_2 background but to a lesser degree. In either case, evacuation of the O_2 results in a partial return to the original state, indicating ESD of some of the adsorpbed O_2 by the ELS primary beam. The effect of an O_2 background on an *undamaged* UHV-fractured sample at $E_p = 500$ eV is similar to that shown in Figs. 10(a) and 10(b) but is much less pronounced. At $E_p = 1500$ eV prior to Ar^+-ion bombardment, there is no O_2 background effect. Although we do not have a specific model to account for these data, the striking effect of O_2 on a bombarded sample indicates that surface oxygen vacancies are involved. These are present, to some extent, as an intrinsic property of the UHV-fractured surface, indicating deviation from "ideal" stoichiometry. We note that the energy of this peak, about 22 eV, is equal to that of a transition from the O $2s$ level to the bottom of the conduction band, as shown in Fig. 1. The essential question is why the creation of oxygen vacancies should affect the cross section for such a transition. We speculate that reduction of the surface generates a highly covalent suboxide of tantalum (possibly TaO_2) and that the covalent bonding results in a slight mixture of O $2s$ and unfilled Ta orbitals. Recently Langell and Bernasek[44] have reported the effects of various oxidation and reduction treatments on the surface ELS of WO_3 and Na_xWO_3 ("sodium tungsten bronze") single crystals. One would expect some similarities between WO_3 and $LiTaO_3$, since the W^{6+} and Ta^{5+} ions are isoelectronic (both materials are largely covalent, of course). Previously, we have noted the similarity in the bombardment-induced Auger line-shape changes in the two systems. Langell and Bernasek[44] find that the energy (and probably also the intensity) of the O $2s \rightarrow$ conduction-band transition is strongly dependent on the oxidation and reduction of the surface for Na_xWO_3 and, to a lesser degree, for WO_3. The remaining structure (Fig. 9), consisting of the sharp 7.7-eV peak and the broader features at ~ 11, 14, and 16.5 eV, must be valence-to-conduction-band transitions. Unfortunately, there are no available band-structure calculations or VUV optical data for $LiTaO_3$.

Ar^+-ion bombardment also results in a loss peak in the 3.1—3.5-eV range, as shown in Fig. 10(c). As for $LiNbO_3$, interference from adjacent structures makes exact determination of the peak position somewhat difficult unless the defect peak is strong. The defect peak appears to be stronger at $E_p = 1500$ eV than at $E_p = 500$ eV, which complicates the detection of surface effects. In contrast to the findings for $LiNbO_3$, an O_2 background ap-

pears to attenuate the $LiTaO_3$ ELS defect peak, as shown in Fig. 10(d). However, O_2 does not entirely remove the defect structure, even in more surface-sensitive spectra obtained at $E_p = 500$ eV. This implies that some, but not all, of the $LiTaO_3$ defect ELS structure involves Li^+-ion vacancies. For the undamaged UHV-fractured samples, $LiTaO_3$ (like $LiNbO_3$) exhibits a weak "intrinsic" defect ELS peak (Fig. 9) which is not removed by an O_2 background. Several defect absorption bands[45,46] in the 2.2–4.6-eV range have been reported for $LiTaO_3$ following various thermal and/or radiation treatments, but the identities of the defects responsible are uncertain. However, a band at $\sim$ 3.3 eV (the "*A* center" of Ref. 45) is close in energy to the ELS peak in the bombarded sample before introduction of O_2. The *A* center is believed[45] to be a Ta^{4+} ion adjacent to an oxygen vacancy, possibly containing a single electron. We have previously associated defects of this general description with the bombardment-induced UPS peak shown in Fig. 7.

D. Annealing experiments

In order to obtain a further understanding of the defects, we have observed the effect of annealing on the ELS of ion-bombarded polished-plate samples. The results are shown in Figs. 11 and 12. One first notes that the spectra of the polished plates after bombardment, Figs. 11(a) and 12(a), are closely similar to those of UHV-fractured samples after similar treatment [see Figs. 8(b), 10(a), and 10(c)]. For $LiNbO_3$, the only significant difference is in the energy of the defect peak, which appears to be $\sim$0.5 eV lower in the plate sample. For $LiTaO_3$, the plate sample shows a more pronounced defect peak than do the fractured specimens at $E_p = 500$ eV. At present, we are not certain whether either of these differences is real or the result of the limited energy resolution. Also, for $LiTaO_3$ the $\sim$22 eV transition, which we have previously ascribed to oxygen vacancies, is less pronounced than in Fig. 10(a). This difference is probably not significant, since the appearance of this part of the $LiTaO_3$ ELS varies somewhat from one UHV-fractured sample to another. However, in comparing Figs. 10(a) and 12(a), we can conclude that the species responsible for the two defect peaks, at $\sim$3.5 and $\sim$22 eV, are probably different.

After a "short" anneal at about 650 °C, the spectra are closely similar to those of UHV-fractured samples at $E_p = 500$ eV [compare Fig. 8(a) with 11(b) and Fig. 9(a) with 12(b)]. The main difference is that some of the features are sharper in the annealed specimens. There is some indication from AES that a "short" anneal diminishes the surface carbide concentration remaining after ion bombardment. However, a "long" anneal leads to rather drastic changes, mainly in the 7–15-eV interband-transition range. These may result from the annealing-induced stoichiometry changes first reported by Courths *et al.*[8] or from the very heavy surface carbon contamination detected in AES after a long anneal.

With regard to the low-energy defect peak, we see that annealing significantly diminishes the in-

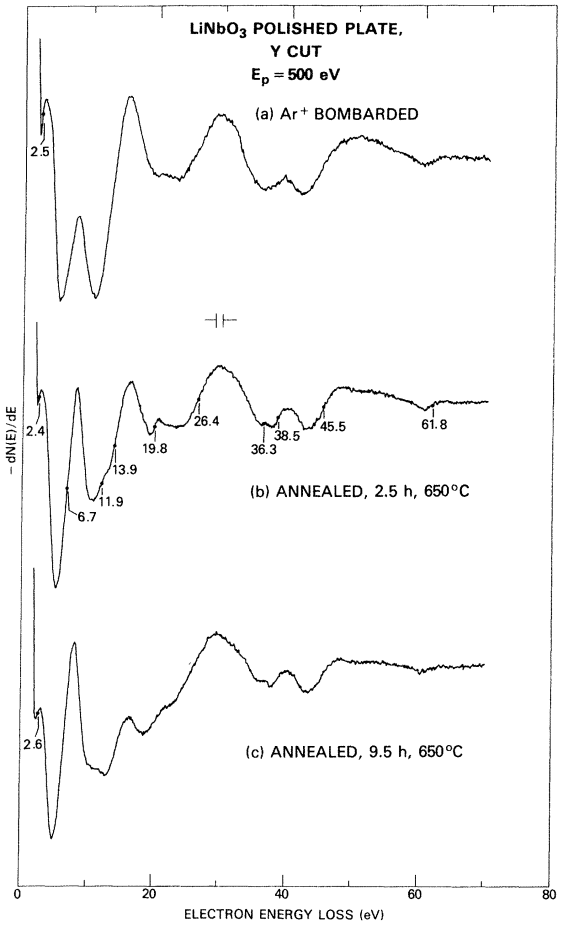

FIG. 11. The effect of annealing on the ELS ($E_p = 500$ eV) of an Ar^+-ion bombarded *y*-cut $LiNbO_3$ polished plate. (a) After bombardment sufficient to reduce surface carbon contamination to $\sim$9 at. %, (b) after a "short" anneal ($\sim 2\frac{1}{2}$ h at 650 °C), (c) after further bombardment [to regenerate (a)] and a "long" anneal ($\sim 9\frac{1}{2}$ h at 650 °C).

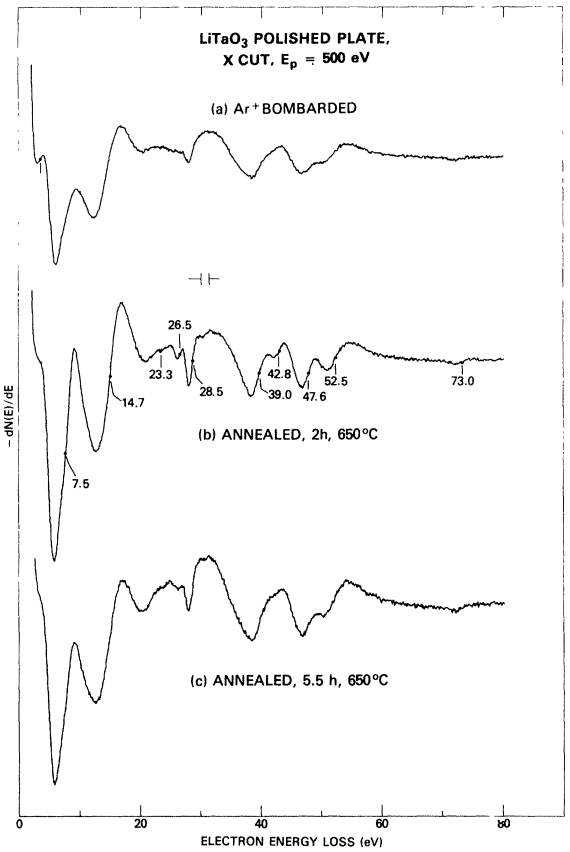

FIG. 12. The effect of annealing on the ELS ($E_p = 500$ eV) of an Ar^+-ion bombarded x-cut $LiTaO_3$ polished plate. (a) After bombardment sufficient to reduce surface carbon contamination to ~ 8 at. %, (b) after a "short" anneal (~ 2 h at 650 °C), (c) after further bombardment [to regenerate (a)] and a "long" anneal ($\sim 5\frac{1}{2}$ h at 650 °C). The defect peak in (a) is at 3.2 eV.

tensity in $LiNbO_3$ and almost eliminates it in $LiTaO_3$. We recall that, at least for $LiNbO_3$, mild annealing causes diffusion of Li_2O out of the bulk, with no detectable (via XPS) reduction in the Nb oxidation state[8] and that an O_2 background has much less of an effect on the defect ELS than does annealing. This indicates that Li^+-ion vacancies are involved in the defects observed in ELS, as was suggested above.

E. Summary and conclusions

The AES of $LiNbO_3$ and $LiTaO_3$ show characteristic line-shape changes following reduction of the UHV-fractured surfaces by Ar^+-ion bombardment. These effects are reversible in an O_2 ambient and can be correlated with variations in the O-to-Nb and O-to-Ta Auger peak-to-peak ratios. The changes result from shifts in the core-level binding energies and/or perturbation of the valence-band local density of states near oxygen vacancies. Freshly fractured surfaces readily accumulate carbon, probably as a result of decomposition of CO in the UHV background, induced by the AES primary electron beam. The *CKLL* line shape indicates a mixture of the carbide and elemental forms of carbon. Ar^+-ion bombardment diminishes the total carbon coverage, but the remaining *CKLL* line shape is distinctly that of a carbide. The impurity probably occupies oxygen vacancies, forming NbC_x or TaC_x ($x < 1$). Ion bombardment of the freshly fractured carbon-covered surface removes elemental carbon in preference to the chemically bound form and/or induces reaction of elemental carbon with the surface by generating oxygen vacancies. After this initial carbon coverage is diminished by Ar^+-ion bombardment, the surface then appears to be "passivated" in that carbon accumulation occurs only at a rate typical for a sample in UHV. Annealing in UHV (~ 650 °C, $\lesssim 2$ h) or electron-beam irradiation at typical AES levels in O_2 further decreases the carbide coverage remaining after ion bombardment.

UPS ($h\nu = 40.8$ eV) data show a bombardment-induced peak at 1.1 ± 0.2 eV above the valence-band edge in $LiNbO_3$ and 1.4 ± 0.2 eV in $LiTaO_3$. An O_2 exposure of about 3×10^4 L virtually eliminates the defect. In agreement with previous work,[8] the defect is described as an M^{4+} – (oxygen vacancy) complex, analogous to those formed in various ion-bombarded titanate materials (Refs. 11–13 and works cited). The electronic structure of this defect is almost certainly more complex than is implied by the simple description given here, as shown in various theoretical treatments[47,48] of similar surface states in TiO_2 and $SrTiO_3$. The valence-band UPS shape is found to change with the introduction of vacancies and/or disorder, in agreement with Courths *et al.*[8]

ELS data have been obtained as a function of primary beam energy and of various oxidation, reduction, and annealing treatments. Several transitions originating in the valence band and upper core levels have been identified. Bulk plasmons have been located at $\hbar\omega_p = 26.0 \pm 0.5$ eV in $LiNbO_3$ and at $\hbar\omega_p = 21.7 \pm 0.5$ eV in $LiTaO_3$, but no surface plasmons were observed. In $LiNbO_3$, a feature

observed at about $2\hbar\omega_p - 6$ eV is tentatively assigned to the excitation of two strongly coupled plasmons. Ar^+-ion bombardment results in a low-energy loss peak at $\sim 2.5-3.0$ eV in $LiNbO_3$ and $\sim 3.1-3.5$ eV in $LiTaO_3$. O_2 adsorption has little effect on the loss intensity in $LiNbO_3$ but causes a noticeable decrease in $LiTaO_3$. Annealing at 650 °C, which causes Li_2O to diffuse out of the bulk, diminishes the defect loss peak in $LiNbO_3$ and almost eliminates it in $LiTaO_3$. Defects removed by annealing but not by O_2 adsorption are believed to involve Li^+-ion vacancies, perhaps in combination with other defects (oxide-ion vacancies, reduced metal ions, etc.). In $LiTaO_3$, a transition at ~ 22 eV, thought to be from the O 2*s* level to the bottom of the conduction band, is observed and found to vary in appearance from one sample to the next (indicating extrinsic effects) and to be dependent on surface oxidation and reduction. Somewhat similar results are found for WO_3.[44] We have tentatively suggested that the oxygen-deficient surface contains a highly covalent suboxide of tantalum (possibly TaO_2, for example) and that mixing of O 2*s* with unfilled Ta levels in a bonding molecular orbital enhances the O $2s \rightarrow$ conduction-band cross section.

The same low-energy defect ELS peaks induced by ion bombardment are also observed, with less intensity, in UHV-fractured samples prior to bombardment. The effect of O_2 on the ~ 22 eV "O 2*s* peak" in $LiTaO_3$, first noted in bombarded samples, is also observed in the surface-sensitive ELS ($E_p = 500$ eV) prior to bombardment but to a lesser degree. Apparently a UHV-fractured surface contains a small intrinsic deficiency of oxygen and lithium. Unfortunately, our system does not include an x-ray source, which would have permitted monitoring changes in the surface Li concentration via the *K*-shell XPS. In our work, lithium Auger lines, generated by interatomic decay of *K*-shell holes, were obscured by the slow-secondary background. We note that the stoichiometry of $LiNbO_3$, which can be expressed formally as $Li_2O + Nb_2O_5$, shows a complicated dependence on the thermal and chemical history of the material,[4] although the $[Li_2O]/[Nb_2O_5]$ concentration ratio is within a few percent of unity for high-quality single crystals. Widely varying compositions [$LiNb_3O_8 = Li_2O + 3(Nb_2O_5)$ and $Li_3NbO_4 = 3(Li_2O) + Nb_2O_5$] are chemically stable. However, simple alteration of the $[Li_2O]/[Nb_2O_5]$ ratio does not involve oxidation or reduction since the Nb remains in the +5 formal oxidation state and no charge-compensating electron or hole traps need be formed in the lattice. On the other hand, the defects observed in UPS and ELS must originate from an actual reduction of the sample, since much of the structure can be diminished or entirely eliminated by exposure to O_2. Some of the low-energy ELS structure in $LiTaO_3$ (and most of it in $LiNbO_3$) does not respond to O_2 adsorption. However, the peaks are narrow, and the energies are less than the optical band gap in either material by at least 0.5 eV, indicating that point defects are involved.

The results obtained here, together with those previously reported,[8] can account for some observations[4] concerning optical damage in these materials. For example, high-temperature processing of high-purity $LiNbO_3$ in vacuum ("vacuum outdiffusion")[4] enhances optical damage. This can be explained in terms of the formation of Nb^{4+}, as reported by Courths *et al.*[8], which can then be photoionized. However, pure $LiTaO_3$ is reported to be much less sensitive to optical damage than is pure $LiNbO_3$. Assuming defects to be the major donor species after thermal processing of high-purity materials in vacuum, this can be explained by the higher defect absorption energy in the tantalate, as found in ELS.

The surface defect properties of these materials, especially $LiTaO_3$, are apparently quite complex. Although our approach has been only qualitative, we have been able to gain some insight into the problem. Further understanding would require a quantitative correlation of the UPS and ELS defect energies and intensities—as functions of ion bombardment, oxidation, and annealing—with changes in stoichiometry and metal-ion oxidation state (as revealed by AES or, preferably, XPS). An example of such an approach is that of Tait and Kasowski[13] and of Henrich *et al.*[49] to TiO_2 and $SrTiO_3$ surface defects.

ACKNOWLEDGMENTS

We are grateful to C. H. Bulmer for helpful discussions leading to the inception of this work. We thank E. J. West for help in some of the sample preparation and J. F. Weller and S. K. Sheem for providing the polished-plate samples.

[1]M. E. Lines and A. M. Glass, *Principles and Applications of Ferroelectrics and Related Materials* (Clarendon, Oxford, 1977).
[2]A. J. Slobodnik, Proc. IEEE 64, 581 (1976).
[3]A. M. Glass, Opt. Eng. 17, 470 (1978).
[4]R. L. Holman, P. J. Cressman, and J. F. Revelli, Appl. Phys. Lett. 32, 280 (1978).
[5]G. M. Zverev, E. A. Levchuk, V. A. Pashkov, and Yu. D. Poryadin. Kvantovaya Elektron. 2, 94 (1972) [Sov. J. Quantum Electron. 2, 167 (1972)].
[6]P. Steiner and H. Höchst, Z. Phys. B 35, 51 (1979).
[7]T. P. Pearsall, S. Chiang, and R. V. Schmidt, J. Appl. Phys. 47, 4794 (1976).
[8]R. Courths, P. Steiner, H. Höchst, and S. Hüfner, Appl. Phys. 21, 345 (1980).
[9]L. Kasper and S. Hüfner, Phys. Lett. 81A, 165 (1981).
[10]V. M. Bermudez and V. H. Ritz, Chem. Phys. Lett. 73, 160 (1980).
[11]S. Ferrer and G. A. Somorjai, Surf. Sci. 94, 41 (1980).
[12]R. Courths, Phys. Status Solidi B 100, 135 (1980).
[13]R. H. Tait and R. V. Kasowski, Phys. Rev. B 20, 5178 (1979).
[14]Crystal Technology Inc., 1035 East Meadow Circle, Palo Alto, California 94303.
[15]I. P. Kaminow, E. W. Turner, R. L. Barns, and J. L. Bernstein, J. Appl. Phys. 51, 4379 (1980).
[16]G. K. Wertheim, Rev. Sci. Instrum. 46, 1414 (1975).
[17]J. C. Fuggle and D. Menzel, Surf. Sci. 74, 321 (1978).
[18]W. A. Coghlan and R. E. Clausing, At. Data 5, 317 (1973).
[19]K. Bärner, R. Braunstein, and H. A. Weakliem, Phys. Status Solidi B 68, 525 (1975).
[20]V. N. Vishnevskii, E. P. Marchuk, Ya. I. Mikhailishin and N. S. Pidzyrailo, Fiz. Tverd. Tela 17, 1780 (1975) [Sov. Phys.—Solid State 17, 1155 (1975)].
[21]E. Wiesendanger and G. Gütherodt, Solid State Commun. 14, 303 (1974).
[22]D. M. Krol, G. Blasse, and R. C. Powell, J. Chem. Phys. 73, 163 (1980).
[23]F. M. Michel-Calendini, H. Chermette, and J. Weber, J. Phys. C 13, 1427 (1980).
[24]Y. Yafet and R. E. Watson, Phys. Rev. B 16, 895 (1977).
[25]J. A. D. Matthew and Y. Komninos, Surf. Sci. 53, 716 (1975).
[26]M. A. Smith, S. Sinharoy, and L. L. Levenson, J. Vac. Sci. Technol. 16, 462 (1979).
[27]R. Holm and S. Storp, Appl. Phys. 12, 101 (1977).
[28]T. T. Lin and D. Lichtman, J. Mater. Sci. 14, 455 (1979).
[29]P. C. Karulkar, J. Vac. Sci. Technol. 18, 169 (1981).
[30]T. T. Lin and D. Lichtman, J. Appl. Phys. 50, 1298 (1979).
[31]D. Baüerle, W. Braun, V. Saile, G. Sprüssel, and E. E. Koch, Z. Phys. B 29, 179 (1978).
[32]R. E. Thomas, A. Shih, and G. A. Hass, Surf. Sci. 75, 239 (1978).
[33]K. Kam, J. H. Henkel, and H. Hwang, J. Chem. Phys. 69, 1949 (1978).
[34]H. Chermette, P. Pertosa, and F. M. Michel-Calendini, Chem. Phys. Lett. 69, 240 (1980).
[35]W. Bollmann and M. Gernand, Phys. Status Solidi A 9, 301 (1972).
[36]M. G. Clark, F. J. DiSalvo, A. M. Glass, and G. E. Peterson, J. Chem. Phys. 59, 6209 (1973).
[37]V. A. Antonov, P. A. Arsenev, B. A. Baranov, N. D. Barinova, E. F. Kustov, and I. G. Linde, Krist. Tech. 9, 1403 (1974).
[38]H. Bernhardt, Phys. Status Solidi A 33, 211 (1976).
[39]L. G. Karaseva, G. P. Bondarenko, and V. V. Gromov, Radiat. Phys. Chem. 10, 241 (1977).
[40]W. Bollmann, Phys. Status Solidi A 40, 83 (1977).
[41]O. F. Schirmer and D. von der Linde, Appl. Phys. Lett. 33, 35 (1978).
[42]M. D. Sturge, H. J. Guggenheim, and M. H. L. Pryce, Phys. Rev. B 2, 2459 (1970).
[43]V. M. Bermudez and D. S. McClure, J. Phys. Chem. Solids 40, 129 (1979); 41, 187 (1980).
[44]M. A. Langell and S. L. Bernasek, Phys. Rev. B 23, 1584 (1981).
[45]V. A. Antonov, P. A. Arsenev, I. G. Linda, and V. L. Farstendiker, Phys. Status Solidi A 28, 673 (1975).
[46]T. Kobayashi, Solid State Commun. 33, 95 (1980).
[47]S. Ellialtioğlu, T. Wolfram, and V. E. Henrich, Solid State Commun. 27, 321 (1978).
[48]M. Tsukada, C. Satoko, and H. Adachi, J. Phys. Soc. Jpn. 47, 1610 (1979); 48, 200 (1980).
[49]V. E. Henrich, G. Dresselhaus, and H. J. Zeiger, Phys. Rev. B 17, 4908 (1978).